

1 **Simulating the transportation and dispersal of volcanic**
2 **ash cloud with initial condition created by 3D plume**
3 **model**

4 **Key Points:**

- 5 • Creating initial conditions for volcanic ash transport and dispersal models based
6 on 3D plume model output eliminates need for assumptions or inversion regarding
7 initial ash particle distribution with height, and improves prediction capability.
8 • Initial particle distribution in vertical direction has greater impact on transport
9 of ash clouds than does horizontal distribution.
10 • Ash particles involved in long-range transport are initially concentrated in the um-
11 brella cloud of large eruptions.
12

13 **Abstract**

14 VATD (volcanic ash transportation and dispersion) models require initial conditions de-
 15 scribing the initial concentration of ash with height. Most VATD models use a line source
 16 of some prescribed shape calibrated against an empirical expression for the height-MER
 17 relation. Such empirical vertical ash distributions may not be good representations of
 18 actual vertical ash distributions, which usually vary from case to case and have complex
 19 dependencies on eruption source parameters and atmospheric conditions. 3D (three-dimensional)
 20 plume models provide an alternative way to create initial ash cloud without any assump-
 21 tion regarding plume geometry. By eliminating assumed behavior associated with the
 22 semiempirical plume geometry, the predict capacity of VATD simulation would be im-
 23 proved. However, no VATD simulation adopts initial condition created from 3D plume
 24 simulation yet. We explore this option for the first time in this paper. A volcanic plume
 25 model based on Lagrangian method is adopted to cooperate with another Lagrangian
 26 VATD model to demonstrate implementation details. The importance of initial condi-
 27 tion is shown in sensitivity analyses which prove that volcanic ash transportation sim-
 28 ulation is much more sensitive to initial condition than all other input parameters. Fur-
 29 ther investigation reveals that initial particle distribution in vertical direction has more
 30 significant impact on transportation of ash clouds than horizontal distribution. Com-
 31 parison also indicates that ash particles are concentrated along intrusion height of um-
 32 brella cloud that is much lower than the plume top, which is just momentum overshoot.

33 **1 Introduction**

34 **1.1 Volcanic Ash Transportation Forecast**

35 The fine-grain fraction of tephra (volcanic ash) can be widely dispersed, and can
 36 lead to a degradation of air quality and pose threats to aviation (?). Identification of vol-
 37 canic ash helps schedule flights to avoid areas where ash is present. Numerical estima-
 38 tion of ash distribution using known and forecast wind fields is necessary if we are to ac-
 39 curately predict ash cloud evolution. Numerous VATD (volcanic ash transportation and
 40 dispersion) models have been developed by both civil and military aviation or meteo-
 41 rological agencies to provide forecasts of ash cloud motion (Witham et al., 2007). New
 42 techniques have been integrated with VATDs to satisfy increasing demands for more out-
 43 puts, model accuracy and forecast reliability. This contribution explores a method for
 44 creating initial conditions for VATD simulations, which promises to improve prediction
 45 capability and accuracy.

46 Fero et al. (2009); ? showed that initial conditions have significant effects on sim-
 47 ulation of volcanic ash transportation. Traditional VATD simulation requires key global
 48 descriptors of the volcanic plumes, especially plume height, grain size, eruption duration
 49 and mass loading, or alternatively, a mass eruption rate (MER). No matter how these
 50 global descriptors are obtained, they are used to furnish the initial conditions for VATDs
 51 in the form of a line-source term of a spatio-temporal distribution of particle mass. It
 52 is a common practice to pick values for these global descriptors using an empirical ex-
 53 pression for the height-MER relation. The empirical expression is written as a function
 54 of several parameters, including the key global descriptors. The values for the descrip-
 55 tors can also be found by parameter calibration (e.g. Fero et al., 2008, 2009; ?; Zidikheri
 56 et al., 2017). 1D plume models serve as an alternative option to provide values. For ex-
 57 ample, Bursik et al. (2012) and Stefanescu et al. (2014) used the 1D model puffin (Bur-
 58 sik, 2001) to generate estimates of mass eruption rate and grain size. In some cases, an
 59 extra step is adopted to spread ash particles from the line source horizontally, resulting
 60 in an initial ash cloud in 3D space. The horizontal spreading depends on an empirical
 61 expression. For example, The VATD model Puff spreads particles from the line source
 62 uniformly in the horizontal direction within a given radius using an empirical expression
 63 or puffin. Considering the complexities of volcanic eruptions, the actual ash distribution

in initial ash clouds should vary from case to case and with time, making it difficult to find one general expression that is suitable for all cases. It is useful therefore to investigate alternative ways for creating initial ash clouds without assumptions regarding plume geometry or numerical inversion. This is one major motivation of this paper.

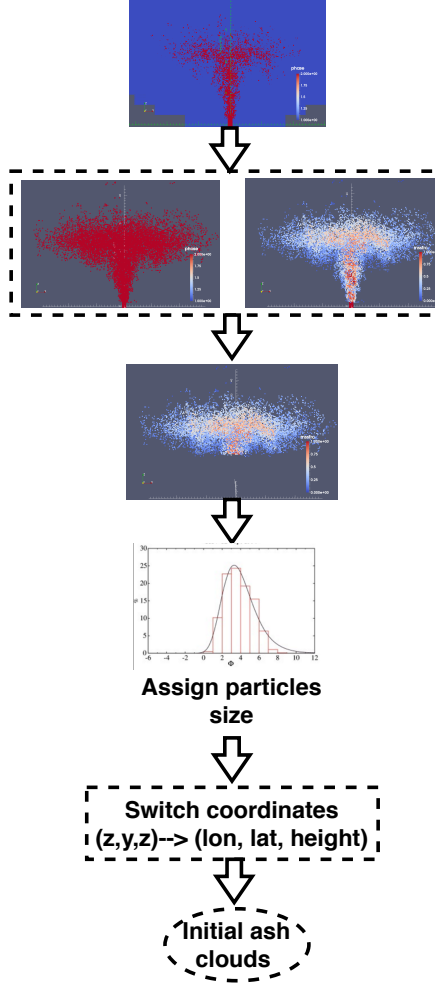
1.2 Numerical Tools

VATD models can be categorized into Lagrangian particle tracking and Eulerian advection-diffusion types. Among several available particle tracking models (e.g. Walko et al., 1995; Searcy et al., 1998; D'amours, 1998; Draxler & Hess, 1998) and advection-diffusion models (e.g. Bonadonna & Houghton, 2005; Folch et al., 2009; Schwaiger et al., 2012), we adopt a particle tracking model, Puff (Tanaka, 1991; Searcy et al., 1998), as the VATD model. Puff can take 3D ash clouds as initial conditions, which makes it technically easier to cooperate with 3D plume models. Puff initializes a discrete number of tracers that represent a sample of the eruption cloud, and calculates transport, turbulent dispersion, and fallout for each representative tracer. A cylinder emanating vertically from the volcano summit to a specified maximum height is the standard approach to crudely model the geometry of a typical ash column. Puff minimally requires horizontal wind field data. The “restart feature” of Puff makes it technically feasible to accommodate the hand-off between a plume simulation and the Puff simulation in terms of time and length scales.

Besides parameter calibration, 1D (one dimensional) plume models have been used to obtain global descriptors of volcanic plumes. 1D plume models (e.g. Woods, 1988; Bur sik, 2001; Mastin, 2007; de'Michieli Vitturi et al., 2015; Folch et al., 2016; Pouget et al., 2016) solve the equations of motion in 1D using simplifying assumptions, and hence depend on estimation of certain parameters, especially those related to the entrainment of air, which is evaluated based on two coefficients: a coefficient due to turbulence in the rising buoyant jet, and one due to the crosswind field. Different 1D models adopt different entrainment coefficients based on a specific formulation or calibration against well-documented case studies. The feedback from plume to atmosphere is usually ignored in 1D models. While these 1D models generated well-matched results with 3D models for plumes that are much influence by wind, often called weak plumes, much greater variability is observed for strong plume scenarios (Costa et al., 2016). On the other hand, 3D numerical models for volcanic plumes based on first principles and having few parametrized coefficients (Oberhuber et al., 1998; Neri et al., 2003; Y. J. Suzuki et al., 2005; Cerninara, Esposti Ongaro, & Berselli, 2016; Cao et al., 2018) naturally create a 3D ash cloud, which could serve directly as an initial state of the volcanic material for VATDs. However, there is no VATD simulation using such 3D ash clouds as initial conditions. In this paper, we will carry out VATD simulations using an initial state for the ash cloud based on 3D plume simulations, generated with Plume-SPH (Cao et al., 2018). The implementation techniques described in this paper can be applied for any combination of VATD model and 3D plume model even though our investigation is based on a specific VATD model and plume model.

1.3 Pinatubo Eruption

The 1991 eruption of Pinatubo volcano is used as a case study. Pinatubo erupted between June 12 and 16, 1991, after weeks of precursory activity. The climactic phase started on June 15 at 0441 UTC and ended around 1341 UTC (R. Holasek et al., 1996). The climactic phase generated voluminous pyroclastic flows, and sent Plinian and co-ignimbrite ash and gas columns to great altitudes (Scott et al., 1996). The evolution of the Pinatubo ash and SO_2 clouds was tracked using visible (R. Holasek et al., 1996), ultraviolet (Total Ozone Mapping Spectrometer; TOMS) (Guo, Bluth, et al., 2004) and infrared sensors, including the Advanced Very High-Resolution Radiometer (AVHRR) (Guo, Rose, et al., 2004). There are also sufficient observational data to estimate the erup-



120 **Figure 1.** Work flow to create initial condition for Puff based on raw output of Plume-SPH.
 121 Top: raw output of Plume-SPH. Blue particles are phase 1 (ambient air), red particles are phase
 122 2 (erupted material). Second row: plume after removing SPH particles of phase 1. Left: colored
 123 according to mass fraction of erupted material. Third row: volcanic plume above the “corner”
 124 region after cutting off lower portion.

115 tion conditions for the climactic phase of the eruption (Y. Suzuki & Koyaguchi, 2009).
 116 The availability of calibrated eruption conditions and extensive observational data re-
 117 garding ash clouds transport make the Pinatubo eruption an ideal case study.

118 2 Setting up Simulations

119 2.1 Creation of Initial Ash Cloud

120 The steps to create an initial ash cloud based on the raw output of Plume-SPH are
 121 shown in Fig. 1. The method proposed consists in generating the initial ash cloud di-
 122 rectly from Plume-SPH, foregoing assumptions and estimates or inverse modeling regard-
 123 ing ash injection height and timing thereof. We use Plume-SPH as an example, noting
 124 that for other 3D plume models, the steps would be similar. Plume-SPH is a two-phase
 125 model based on the Lagrangian smoothed-particle hydrodynamics (SPH) method, in which
 126 the computational domain is discretized by SPH particles. The current version, Plume-

SPH 1.0 (Cao et al., 2018), uses two types of SPH particles: 1) particles of phase 1 to represent ambient air, and 2) particles of phase 2 to represent erupted material. The initial ash cloud is created from SPH particle of phase 2.

After reaching the maximum rise height and starting to spread horizontally, particles of phase 2 form an initial umbrella cloud (Fig. 2). The 3D plume simulation is considered complete once the umbrella cloud begins to form. Parcels that will be transported by the ambient wind are those above the “corner” region, where mean plume motion is horizontal rather than vertical.

Considering that SPH particles are only discretization points, each is assigned a grain size according to a given total grain size distribution (TGSD) (Paladio-Melosantos et al., 1996), and a concentration according to the mass and volumetric eruption rate. The Plume-SPH discretization points are thus switched to Puff Lagrangian tracer particles having grain sizes and concentrations. The coordinates of these tracer particles, which are initially in the local Cartesian coordinate system of Plume-SPH, are converted into Puff’s global coordinate system, which is given in terms of (*longitude, latitude, height*). Puff takes the initial ash cloud, consisting of the collection of Lagrangian tracer particles with grain size and concentration, and propagates from time t to time $t + \Delta t$ via an advection/diffusion equation (Searcy et al., 1998).

$$\mathbf{R}_i(t + \Delta t) = \mathbf{R}_i(t) + \mathbf{W}(t)\Delta t + \mathbf{Z}(t)\Delta t + \mathbf{S}_i(t)\Delta t \quad (1)$$

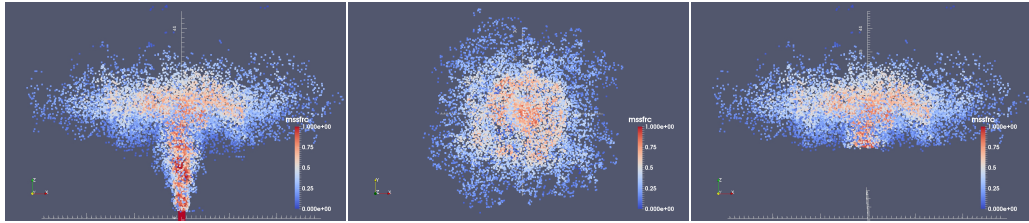
Here, $\mathbf{R}_i(t)$ is the position vector of the i^{th} Lagrangian tracer particle at time t , \mathbf{W} accounts for wind advection, \mathbf{Z} accounts for turbulent dispersion and \mathbf{S} is the terminal gravitational fallout velocity, which depends on tracer’s size.

To summarize, there are four steps to create an initial ash cloud from the raw output of Plume-SPH:

1. filter by SPH particle type to select SPH particles that represent erupted material (phase 2)
2. filter by a mean velocity threshold to select the upper part (above the “corner” region) dominated by horizontal transport
3. switch SPH discretization points to Lagrangian tracer particles, by assigning grain size to each particle
4. convert coordinates of the SPH Lagrangian tracers into the VATDs’ geographic coordinate system

The features of the volcanic plume and resulting initial ash cloud used in the case study are shown in Fig. 2. It is important to point out that since both Plume-SPH and Puff are based on the Lagrangian method, there is no extra step of conversion between an Eulerian grid and Lagrangian particles.

Table 1 compares three different methods for creating initial conditions for VATD simulation: 1) creating initial condition based on parameter calibration without any plume model (method 1), 2) creating initial condition based on output of 1D plume model (method 2), 3) extracting initial ash cloud from 3D plume simulation (method 3). The first method determines all global descriptors of volcanic plume based on calibration. Then create initial line source or ash cloud according to semiempirical plume shape expression. Both other two methods depend on plume models. However 3D plume models can generate initial ash cloud in 3D space while 1D plume models only obtain global descriptors of plume so still need semiempirical expression to create 3D initial ash cloud. In addition, the number of Lagrangian tracers is a free parameter when using semiempirical plume shape expressions while it purely depends on simulation when creating initial condition from 3D plume simulation results.



168 **Figure 2.** All particles in the pictures are of type phase 2 (phase 1 has been removed in step
 169 1) at 600s after eruption, at which time, the plume has already reached the maximum height
 170 and started spreading radially. Pictures from left to right are: front view of the whole plume,
 171 top view of the plume and front view of the initial ash cloud, which is essentially portion of the
 172 whole plume with elevation higher than a given threshold (in this picture is 15000m). Particles
 173 are colored according to mass fraction of erupted material. Red represents high mass fraction
 174 while blue represents low mass fraction.

187 **Table 1.** Three different methods for creating initial conditions (initial ash clouds) for Puff
 188 simulation

	No model	1D model	3D model
Maximum height	Calibration	Semiempirical	1st principle
Average height	Calibration	Conservation laws (1D)	1st principle
Vertical spread	Calibration	Semiempirical	1st principle
Column radius	Calibration	Conservation laws (1D)	1st principle
Plume shape	Semiempirical	Semiempirical	1st principle
Tracers number	Free parameter	Free Parameter	Based on simulation

189 2.2 Puff Restart

190 The plume and ash transport models are run at different time scales and length
 191 scales. The spatial and temporal resolutions of the plume simulations are much finer than
 192 those of the ash transport model. It takes tens of minutes (600s in this case) for the Pinatubo
 193 plume to reach a steady height. However the eruption persisted for a few hours (9 hours
 194 for the climactic phase of Pinatubo eruption), and it may be necessary to track ash trans-
 195 port for days following an eruption. At present, it is too expensive computationally to
 196 do 3D plume simulations of several hours in real time. In order to handle the difference
 197 in time scale, we mimic a continuing eruption with intermittent pulsed releasing of ash
 198 particles. Particularly, we restart Puff at an interval of 600s, i.e., the physical time of
 199 the plume simulation to reach steady height. At every Puff restart, we integrate the out-
 200 put of the last Puff simulation and Plume-SPH into a new ash cloud. This new ash cloud
 201 serves as a new initial condition with which to restart a Puff simulation. The interval
 202 of the pulsed releases is the simulation time of Plume-SPH, i.e., 600s in our case study.
 203 A sketch demonstrating the overall restart process is shown in Fig. (3). The total num-
 204 ber of Lagrangian tracer particles used in Puff thus equals the summed number of par-
 205 ticles in all releases. So the total number of tracer particles is no longer a user-selected
 206 parameter. Fero et al. (2008) proposed using more realistic time-dependent plume heights.
 207 We do not adopt that strategy here for simplicity, although the idea would be straight-
 208 forward in execution.

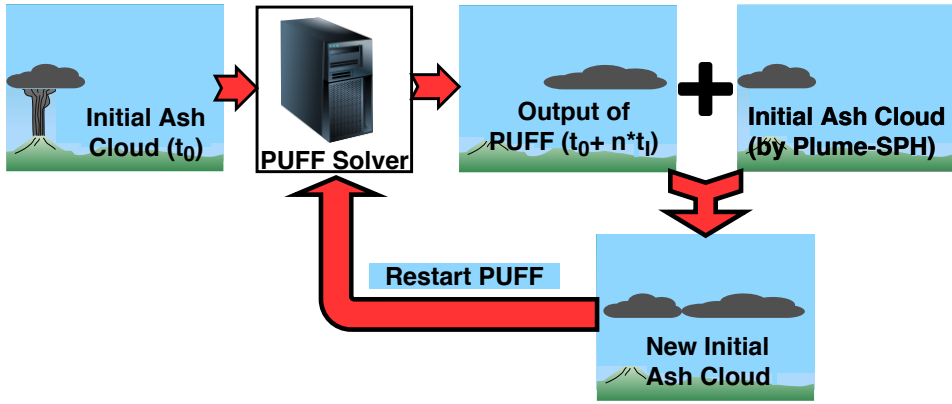


Figure 3. Mimic successive eruption with intermittent pulsing releasing of ash particles. t_I is the period of pulsing release. t_I equals to physical time of 3D plume simulation.

2.3 Sensitivity Analysis of Other Parameters

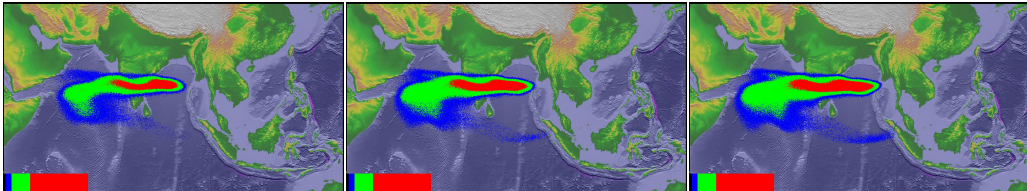
Besides the positions of particles in the initial ash cloud, other parameters for Puff simulations are: horizontal diffusivity, vertical diffusivity, mean grain size, grain size standard deviation and total number of tracers. We present in this subsection systematic sensitivity studies on these parameters. We also investigate the influence of eruption duration. The sensitivity analyses will serve as the basis for identifying possible sources of disparities between simulation and observation.

The sensitivity analyses illustrate that adjustment of other parameters produces negligible visual differences in VATD simulation results. Using different vertical diffusivities in range of $[100, 100000] m^2 s^{-1}$ and different horizontal diffusivities in range of $[1, 20] m^2 s^{-1}$ produces visually negligible differences. The simulation eruption duration should depend on the total observed duration or the duration of the climactic phase. We conducted several simulations with eruption duration varying in range of $[5, 11] hours$ with slight different starting time of climactic phase. Table 2 lists all these simulations. However, only tiny visible differences are observed among the simulated ash transportation. The mean of grain size also has visually ignorable effects on long-term ash transportation according to our sensitivity tests varying the log mean (base 10) grain radius in a range of $[-7.3, -3.5] m$. The standard deviation, when varying in range of $[0.1, 10]$, generate ignorable difference on long-term ash transportation as well. Similar conclusion on parameter sensitivity is reported by Fero et al. (e.g. 2008); Daniele et al. (e.g. 2009). Among these parameters, the eruption duration and beginning time shows, even though tiny, the most obvious influence on simulated ash distribution. In order to show such differences in an intuitive way, Fig. 2 shows simulated ash distribution corresponding to 4.9 hours duration, 9 hours duration and 11 hours duration respectively. After 72 hours, relative to the simulation starting time, these three cases generate generally similar results, with high concentration ash covers almost the same region. The difference of lower concentration distribution is relatively more obvious. Ash cloud covers broadest area when eruption duration is 11.1 hours. To summarize, all these parameters have either tiny or ignorable affects on long-term ash distribution simulation.

The new methodology for generating initial ash cloud introduces another new parameter: elevation threshold. We also carry out sensitivity analysis on this parameter by varying the elevation threshold from $1500 m$ (the height of the vent) to $25000 m$. The simulated ash distributions show obviously visible differences. Such influence is especially obvious when the elevation threshold is either very large or very small. However, varying the elevation threshold in the range of $[12000, 18000] m$ generates relatively small dif-

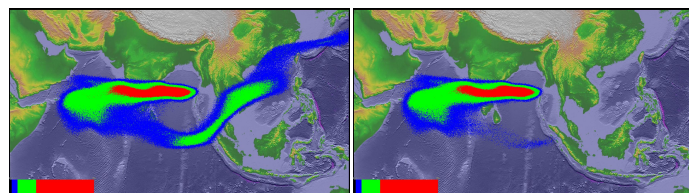
240 **Table 2.** The starting and ending time (UT) for simulating the climactic phase of Pinatubo
 241 eruption on June 15 1991. Observed plume height (R. Holasek et al., 1996) at different time are
 242 also list in the table.

Eruption duration	4.9 hours	9 hours	10 hours	11.1 hours
Start time	0441	0441	0441	0334
Height at start time	37.5 km	37.5 km	37.5 km	24.5 km
End time	0934	1341	1441	1441
Height at end time	35 km	26.5 km	22.5	22.5 km



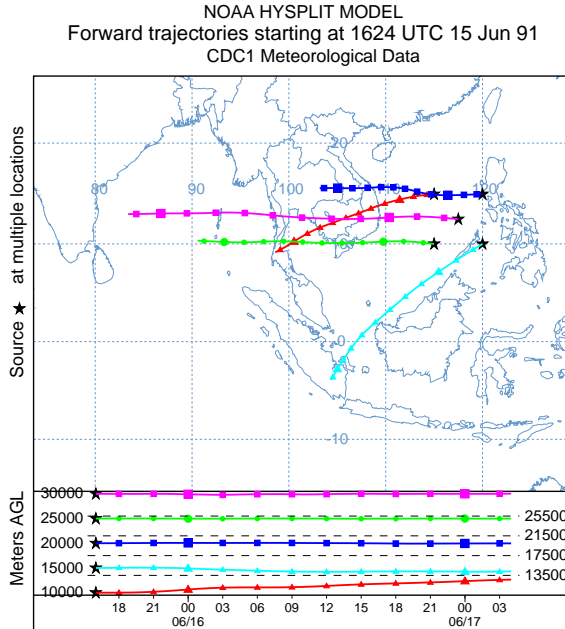
243 **Figure 4.** Simulated ash cloud distribution corresponding to eruption duration of 4.9 hours, 9
 244 hours and 11.1 hours (from left to right) respectively. Starting and ending time for each case is in
 245 Table 1. The contours are for ash distribution at 72 hours after eruption.

252 ference in ash transportation simulation results. Figure 5 compares the simulated ash
 253 distribution corresponding to elevation thresholds of 1500m and 15000m. Compared with
 254 ash distribution for threshold of 15000m, an extra long tail appears when using eleva-
 255 tion threshold of 1500m. Adopting smaller elevation thresholds essentially adds more trac-
 256 ers at lower elevation. As the wind at different elevations are different, these tracers at
 257 lower elevation would transpose to different directions. The forward trajectories, which
 258 starting at June 15 1624 UTC, indicates that the wind between evaluation 10000 m to
 259 15000 m blows from north-east to south-west while wind of higher evaluation blows from
 260 east to west.



261 **Figure 5.** Simulated ash distribution taking initial ash clouds obtained using different el-
 262 evation thresholds (1500m and 15000 m) from output of Plume-SPH. The contours are cor-
 263 responding to ash concentration at 72 hours after eruption. The starting and ending time are
 264 corresponding to 9 hours duration case in Table 2

267 The sensitivity analyses demonstrate that the initial condition for VATD simula-
 268 tion has the most significant effect on simulated ash distribution while all other input
 269 parameters have either tiny or ignorable influence. The initial ash cloud generated based
 270 on semiempirical expression, which is a function of several parameters, might be signif-
 271 icantly disparate from realistic ash cloud. Such initial condition might greatly compro-
 272 mize the accuracy of VATDs simulation.



265 **Figure 6.** Trajectories of particles starting from different heights indicating the wind direction
266 of different evaluations.

273 We do not carry out any investigation with respect to wind field even though it is
274 another dominant factor in VATD simulation. In the case study, we use global *NOAA/OAR/ESRL6–*
275 h , 2.0° reanalysis wind fields data (Whitaker et al., 2004; Compo et al., 2006, 2011).

276 3 Comparison and Discussion

277 Transportation of volcanic ash resulted from Pinatubo eruption on June 15th 1991
278 is simulated using two different initial conditions. The initial condition is created in tra-
279 ditional way according to key global descriptors and semiempirical plume shape expres-
280 sion. The second initial condition is created by the new method proposed in this paper.
281 Simulated ash transportation results are compared against observation.

283 To create initial condition using the new method described in this paper, the plume
284 raising up process is simulated first by Plume-SPH. The eruption parameters, material
285 properties and atmosphere for the strong plume no wind case in a comparison study on
286 eruptive column models (Costa et al., 2016) are adopted. Eruption conditions and ma-
287 terial properties are listed in Table 3. Note that the density of erupted material at the
288 vent and radius of the vent can be computed from the given parameters. The eruption

282

Table 3. List of eruption condition and material properties for plume simulation

Parameters	Units	Plume
Vent velocity	$m \cdot s^{-1}$	275
Vent gas mass fraction		0.05
Vent Temperature	K	1053
Vent height	m	1500
Mass discharge rate	$kg \cdot s^{-1}$	1.5×10^9
Specific heat of gas at constant volume	$J \cdot kg^{-1} \cdot K^{-1}$	717
Specific heat of air at constant volume	$J \cdot kg^{-1} \cdot K^{-1}$	1340
Specific heat of solid	$J \cdot kg^{-1} \cdot K^{-1}$	1100
Specific heat of gas at constant pressure	$J \cdot kg^{-1} \cdot K^{-1}$	1000
Specific heat of air at constant pressure	$J \cdot kg^{-1} \cdot K^{-1}$	1810
Density of air at vent height	$kg \cdot m^{-3}$	1.104
Pressure at vent height	Pa	84363.4

289

pressure is assumed to be the same as pressure of ambient at the vent and hence is not given in the table. The vertical profiles of atmospheric properties were obtained based on the reanalysis data from ECMWF (European Centre for Medium-Range Weather Forecasts) for the period corresponding to the climactic phase of the Pinatubo eruption. The initial ash cloud is obtained by processing the raw output of Plume-SPH following steps described in Sec. 2.

290

291

292

293

294

Another set of initial condition is created based on observed top height (40km) and several other parameters assigned semiempirically (Bursik et al., 2012). These parameters, namely, the global descriptors of volcanic plume, are used as parameters of semiempirical expression to get ash cloud in 3D space. See details in Table 4. Except for initial condition, the simulation parameters that control VATD simulation are the same for both simulations. As has been shown in sensitivity analyses section, these parameters have less influence on simulation results than initial condition.

295

296

297

298

299

300

301

3.1 “Plume-SPH + Puff” and “Semiempirical Initial Cloud + Puff”

306

The simulation results using different initial conditions are compared with TOMS images and AVHRR BTD ash cloud map in Fig. 7.

318

319

320

321

322

323

324

325

326

327

328

329

330

331

332

333

334

The differences between simulated ash transportation by “Semiempirical initial cloud +Puff” and “Plume-SPH+Puff” are obvious. The simulated ash concentration based on initial condition created from Plume-SPH is much closer to observation than that based on semiempirical plume shape expression. Around 23 hours and 31 hours after the beginning of the climactic phase, “Plume-SPH + Puff” simulation generates ash images that generally close to observational image, especially the location where high concentration ash presents. However, these ash at near west to Pinatubo mountain observed in satellite images does not show up in “Plume-SPH + Puff” simulation results. This disparity is very possible due to the fact that the Mountain Pinatubo continued erupting after climactic phase while our simulation only simulates the climactic phase. The ash released after climactic phase is not accounted in our simulation results. The “Semiempirical initial cloud + Puff” simulation, however, forecasts an ash distribution faster and narrower than observation. The location, where the high concentration ash presents, locates to the far northwest of observed ash. Around 55 hours after the beginning of the climactic phase, the disparity between observation and simulation becomes more obvious. Ash distribution of “Semiempirical initial cloud + Puff” simulation locates far west to the observed ash. The high concentration area of “Plume-SPH + Puff” simulation,

302 **Table 4.** Parameters used in VATD simulation of the climactic phase of Pinatubo eruption on
 303 June 15 1991. The first six parameters are used by semiempirical expression to create initial ash
 304 cloud. When create initial condition based on Plume-SPH model, these parameters are extracted
 305 from output of Plume-SPH model.

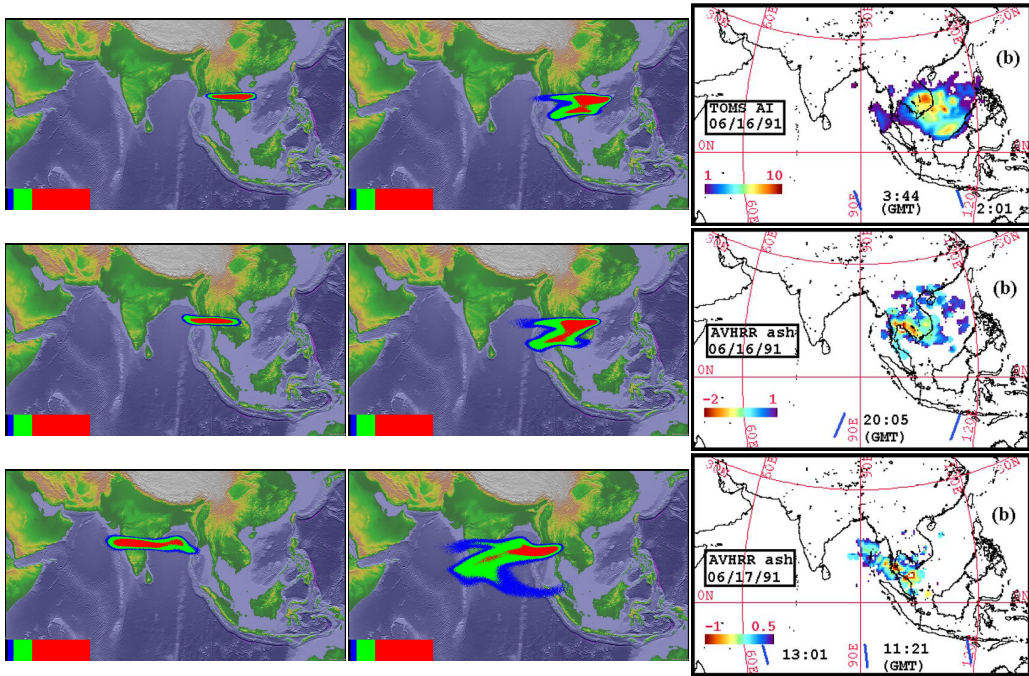
Parameters	Unit	Semiempirical	Plume-SPH
Maximum Height (H_{max})	m	40000	41800
Horizontal Spread (R_{max})	km	103.808	-
Vertical Spread (H_{width})	km	6.662	-
Plume Shape	-	Poisson	-
Total Ash Particles	-	1768500	1768500
Elevation Threshold	m	-	15000
Horizontal Diffusivity	m^2/s	10000	10000
Vertical Diffusivity	m^2/s	10	10
Grain Size Distribution	-	Gaussian	Gaussian
Mean of Grain Size (Radius)	mm	3.5×10^{-2}	3.5×10^{-2}
Standard Deviation of Grain Size	-	1.0	1.0
Start Time	UT	0441	0441
End time	UT	1341	1341
Simulation Duration	hour	72	72

335 even though closer to observation than that of “Semiempirical initial cloud +Puff”, is
 336 still faster than observation.

337 At the stage of ash transportation simulation, except for the initial condition, both
 338 simulations adopt the same parameters and wind field data. That is to say, the only dif-
 339 ference between these two simulations is the initial condition. Recall the initial condi-
 340 tion has most significant influence on ash transportation simulation. It is very possible
 341 that the big difference between simulation results by “Plume-SPH+Puff” and “Semiem-
 342 pirical initial cloud +Puff” is attribute to the initial condition. The ash transportation
 343 simulation based on 3D plume simulation results is much more accurate than that based
 344 on semiempirical initial cloud.

345 3.2 Discussion Regarding Maximum Height (H_{max})

346 In this section, we mainly discuss the vertical distribution of ash particles in ini-
 347 tial ash cloud. The majority of volcanic ash particles usually present a lower elevation
 348 than maximum height. For instance, R. Holasek et al. (1996); R. E. Holasek et al. (1996)
 349 reported the maximum Pinatubo plume height as high as around 39km while the cloud
 350 heights were estimated at 20 ~ 25km, Self et al. (1996) report the maximum plume height
 351 could be > 35km and the plume heights are 23 ~ 28km after 15 ~ 16 hours. The neu-
 352 tral buoyant regions of the Pinatubo aerosol estimated by different measurements are:
 353 17 ~ 26km (lidar) by DeFoor et al. (1992), 20 ~ 23km (balloon) by Deshler et al. (1992),
 354 17 ~ 28km (lidar) by Jäger (1992), and 17 ~ 25km (lidar) by Avdyushin et al. (1993).
 355 Based on comparison between simulated cloud with early infrared satellite images of Pinatubo,
 356 Fero et al. (2008) reported that the majority of ash was transported between 16km and
 357 18km. This is physically understandable as particles are concentrated along intrusion
 358 height of umbrella cloud, not near top because the plume top is due to momentum over-
 359 shoot. However, the empirical expressions for the height-MER relation, which are com-
 360 monly adopted to create initial conditions for VATD simulation, tends to place major-
 361 ity of ash particles closer to top if use observed maximum height in the empirical expres-
 362 sions.



309 **Figure 7.** Comparison between “Semiempirical initial cloud + Puff” and “Plume-SPH +
 310 Puff”. Pictures from left to right are: Puff simulation based on initial condition created according
 311 to semiempirical plume shape expression, Puff simulation based on initial condition generated by
 312 Plume-SPH, TOMS or AVHRR image of Pinatubo ash cloud. Ash clouds at different hours after
 313 eruption are on different rows. From top to bottom, the images are corresponding to around 23
 314 hours after eruption (UT 199106160341), 31 hours after eruption (UT 199106161141), 55 hours
 315 after eruption (UT 199106171141). The observation data on the first row are TOMS ash and ice
 316 map. The observation data on the second and third row are AVHRR BTD ash cloud map with
 317 atmospheric correction method applied (Guo, Rose, et al., 2004).

363 Here we check two commonly used plume shapes, the Poisson and Suzuki. For Pois-
 364 son plume shape, the vertical height of ash particles are determined according to Eq. (2).

$$H = H_{max} - 0.5H_{width} * P + H_{width}R \quad (2)$$

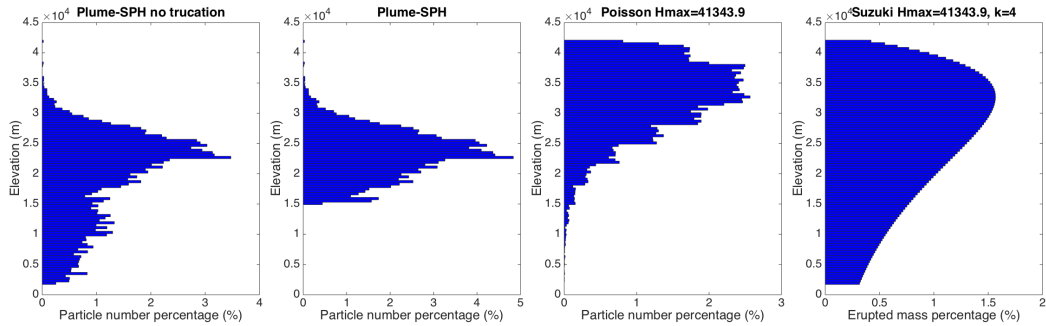
365 where P is an integral value drawn from a Poisson distribution of unit mean, R is a uni-
 366 formly distributed random number between 0 and 1, H_{max} is the maximum plume height,
 367 H_{width} represents an approximate vertical range over which the ash will be distributed.
 368 For Suzuki plume shape (T. Suzuki et al., 1983), volcano ash mass vertical distribution
 369 is assumed to follow the Suzuki equation (Eq. (3)).

$$Q(z) = Q_m * \frac{k^2(1 - z/H_{max})\exp(k(z/H_{max} - 1))}{H_{max}[1 - (1 + k)\exp(-k)]} \quad (3)$$

370 Where Q_m is the total mass of erupted material, k is shape factor, which is an adjust-
 371 able constant that controls ash distribution with height. A low value of k gives a roughly uni-
 372 form distribution of mass with elevation, while high values of k concentrate mass near
 373 the plume top.

374 Particle distribution (in terms of mass percentage or particle number percentage)
 375 in vertical direction in the initial ash cloud are shown in Fig. 8. In that figure, the ver-
 376 tical particle distribution based on Plume-SPH output is compared with vertical par-
 377 ticle distribution created based on semiepirical shape expressions. Both Poisson and Suzuki

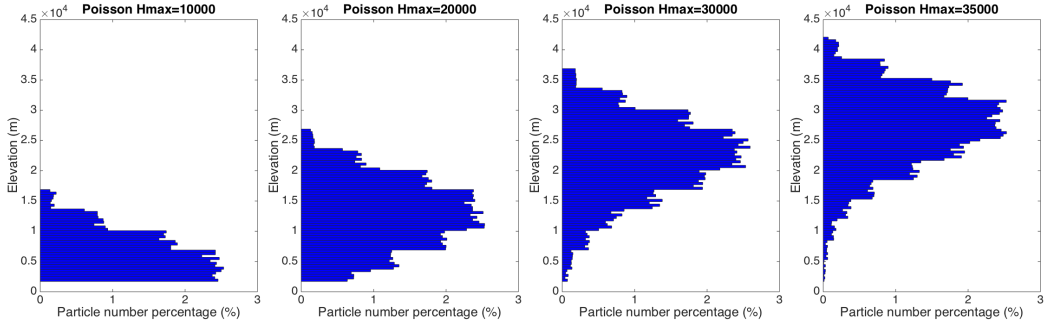
378 distribution in Fig. 8 take $H_{max} = 40000m$, which is close to reported observation of
 379 maximum height. When adopting Poisson plume shape, the majority of the particles are
 380 between $30km \sim 40km$. Obviously, Poisson distributes majority ash at a much higher
 381 elevation than observations (e.g. Fero et al., 2008). As for Suzuki, the majority of ash
 382 particles also distribute in a range that significantly higher than $25km$. As for initial ash
 383 cloud based on Plume-SPH simulation, the major population of ash particles distribute
 384 between $17km \sim 28km$, which match well with observations. The maximum height is
 385 also consistent with observation. To summarize, using semiempirical plume shape ex-
 386 pression generates unrealistic initial ash cloud even if we use observed plume maximum
 387 height.



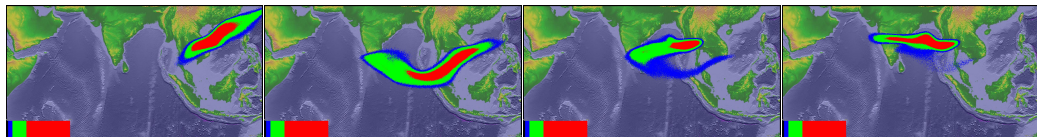
388 **Figure 8.** Particle distribution of initial ash cloud in vertical direction. The picture to the
 389 left is corresponding to initial ash cloud obtained from Plume-SPH output. The second picture
 390 is corresponding to ash distribution truncated by a elevation threshold of $15000m$. The third
 391 picture is for vertical ash distribution based on Poisson distribution with maximum height equals
 392 to $40000m$. Another parameter, the vertical spread, in the expression of Poisson plume shape is
 393 $6662m$. The picture to the right is corresponding to Suzuki distribution with maximum height
 394 equals to $40000m$. Another parameter in Suzuki distribution, the shape factor, is 4. The x axis is
 395 the percentage of particle number for Plume-SPH and Poisson. For Suzuki the x axis is the mass
 396 percentage of erupted material.

397 For Poisson and Suzuki plume shape, vertical distribution of ash particles can't be
 398 lower down without changing the maximum height. To distribute major population of
 399 ash particles at lower elevation, the maximum height has to be reduced to a value smaller
 400 than observed maximum height. Adjusting parameters such as maximum height in the
 401 emperical expression is actually the traditional source term calibration method. A set
 402 of initial ash clouds using different maximum heights based on Poisson plume shape is
 403 shown in Fig. 9). The maximum heights adopted in plume shape expressions are, by no
 404 means, obtained from any plume model or observation. Except for maximum height, all
 405 other parameters for creating initial ash cloud are the same as these in Table 4. The range,
 406 between which major populations of ash particles locate, is lower when using smaller max-
 407 imum heights. These ash clouds created by Poisson distribution with different maximum
 408 heights are then used as initial condition in Puff simulation, whose results are show in
 409 Fig. 10.

420 Figure 10 shows that the maximum height has significant influence on ash trans-
 421 portation simulation. When the maximum height is $10000m$ the high concentration area
 422 is lag behind observation. While the designated maximum height is $35000m$, the high
 423 concentration area is a little bit faster and much narrower than observation. When us-
 424 ing maximum height of $41343.9m$, the high concentration area is faster and narrower than
 425 both observation and “Pume-SPH+Puff” simulation results (see Fig. 7). The simulated
 426 high concentration area is closest to “Pume-SPH+Puff” simulation results when assign-



410 **Figure 9.** Initial particle distribution in vertical direction based on Poisson plume shape with
 411 different maximum heights. Pictures from left to right are corresponding to maximum height of
 412 10000m, 20000m, 30000m, 35000m. Another parameter, the vertical spread, in the expression of
 413 Poisson plume shape is 6662m for all cases. The x axis is the percentage of particle number. See
 414 Fig. 8 for vertical ash distribution of Plume-SPH output.



415 **Figure 10.** Ash transportation simulated by Puff using different initial ash cloud created ac-
 416 cording to Poisson distribution with different maximum heights. Pictures from left to right are
 417 corresponding to maximum plume heights of 10000m, 20000m, 30000m and 35000m. All images
 418 are for simulated ash transportation around 55 hours after eruption (UT 199106171141). See the
 419 observed cloud image in Fig. 7.

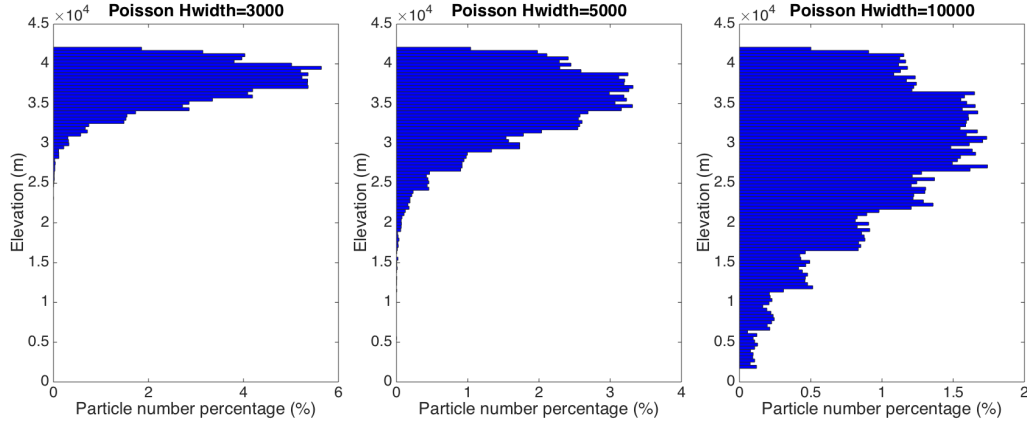
427 ing a maximum height of 30000m. The front of volcano ash, with lower concentration
 428 is faster than observation locating far west to high concentration area. A lower concen-
 429 tration tailing area also appears in the simulation results while there is no such tail in
 430 observed image. Puff simulation result based on calibrated maximum height of 30000m
 431 shows similar footprint to, even though smaller in terms of covered area than, those of
 432 "Pume-SPH+Puff" simulation. However, the initial ash cloud created by Poisson dis-
 433 tribution with maximum height around 20000m generates best match ash distribution
 434 with observation. That is to say, a maximum height lower than real maximum height
 435 is required by Poisson plume shape to distribute ash particles at the same elevation as
 436 real ash distribution. This is physically understandable as maximum plume heights are
 437 reached due to overshoot. Our hypothesis regarding the sources of disparity between "Semiem-
 438 pirical initial cloud +Puff" simulation and observation is confirmed. Since the initial con-
 439 dition has so dominant effect on VATD simulation, it is critical the forecast capability
 440 of VATD simulation to explore the more accurate and adaptive ways for establishing the
 441 initial conditions, especially the method that does not rely on "post event" parameter
 442 calibration.

443 3.3 Discussion Regarding Vertical Spread (H_{width})

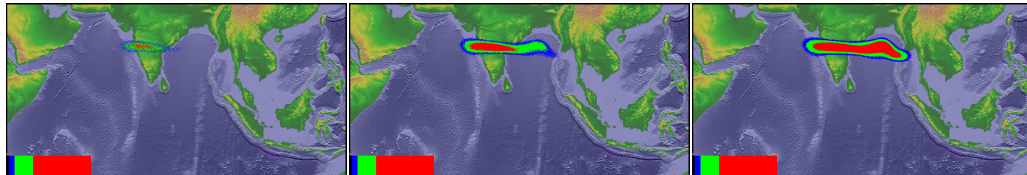
444 In previous section, the maximum height is adjusted to change vertical ash distri-
 445 bution along the source line. This section investigates another parameter in semiempir-
 446 ical poisson expression. We vary the "vertical spread" (H_{width}) in range 3km/ 10km.
 447 A set of initial ash clouds created according to different "vertical spread" is shown in Fig.
 448 11. Except for "vertical spread", all other parameters for creating initial ash cloud are
 449 the same as these in Table 4. Width of the range within which major populations of ash

450 particles locate become narrower when a smaller value for vertical spread is used. But
 451 changing H_{width} has no obvious affect on the height at which majority of ash particles
 452 distribute. These ash clouds based on different vertical spread are then used as initial
 453 condition in Puff simulation, whose results are show in Fig. 12.

454 Adjusting of the vertical spread can change particle distribution in vertical direction
 455 and not surprisingly affect VATD simulation results. Unluckily, none of these VATD
 456 simulations based on initial ash cloud with vertical spread equals to 3km, 5km, and 10km
 457 get better results than VATD simulation based on initial condition created by a 3D plume
 458 simulation using Plume-SPH (see Fig. 12).



459 **Figure 11.** Vertical particle distribution based on Poisson plume shape with different “ver-
 460 tical spread”. Pictures from left to right are corresponding to vertical spread of 3km, 5km and
 461 10km. The maximum height in the expression of Poisson plume shape is 40000m for all cases.
 462 The x axis is the percentage of particle number. See Fig. 8 for vertical ash distribution of Plume-
 463 SPH output.



464 **Figure 12.** Ash transportation simulated by Puff using different initial ash cloud created with
 465 different vertical spread. Pictures from left to right are: Puff simulation results based on initial
 466 ash clouds with vertical spread equals to 3000mm, 5000mm and 10000m. The images are corre-
 467 sponding to around 55 hours after eruption (UT 199106171141). See the observed cloud image in
 468 Fig. 7. The simulated ash field does not adequately cover the observed ash field.

469 The calibrations carried out here are definitely not exhaustive. One might do more
 470 comprehensive calibration throughout the multi-dimensional parameter space (for Pois-
 471 son distribution, the parameter space is two dimension) and get better matched ash trans-
 472 portation results. With more complicated plume shape expression, one could have more
 473 control over plume shape and might be able to get initial condition that much closer to
 474 actual initial ash cloud, hence obtain more accurate ash transportation prediction. But
 475 more complicated plume shape expression usually leads to higher dimensional param-
 476 eter space which requires more effort to do calibration. Even though, the degree of free-

dom to adjust plume shape is still limited. The new method for creating initial conditions based on 3D plume simulation is more adaptive to various cases and obviates semiempirical expressions regarding plume shape.

3.4 Horizontal Ash Distribution

The differences between assumed plume particle distribution and actual (or simulated by 3D plume) model are not only in vertical direction. How cloud horizontal particle distribution of the initial ash cloud affect ash transportation is investigated in this section. Puff uses a uniformly distributed random process to determine the ash particle location in a circle centered on the volcano site. The maximum radius (at top) is given as “horizontal spread” in Table 4. The horizontal displacement from a vertical line above the volcano is a random value within a circle of radius, which equals to “horizontal spread” multiplied by the ratio of the particle height H to maximum H_{max} . So the net shape of the plume is an inverted cone where particles are located directly over the volcano at the lowest level and extend out further horizontally with increasing plume height. As for output of Plume-SPH, an effective radius is determined according to a given threshold of ash concentration following Cerminara, Esposti Ongaro, & Neri (2016). A time averaging and spatial integration of the dynamic 3D flow fields are conducted to get rid of significant fluctuations in time and space. Fig. 13 compares radius of initial ash clouds created by 3D plume simulation and assumed plume shape expression adopted in Puff. Obviously, there is no chance for these two radius to be similar. Adjusting the parameter “horizontal spread” could not make the assumed plume shape to be similar to ash cloud created by Plume-SPH. That is to say, merely parameter calibration is not enough for such situation. It would require higher order semiempirical expression that takes more parameters.

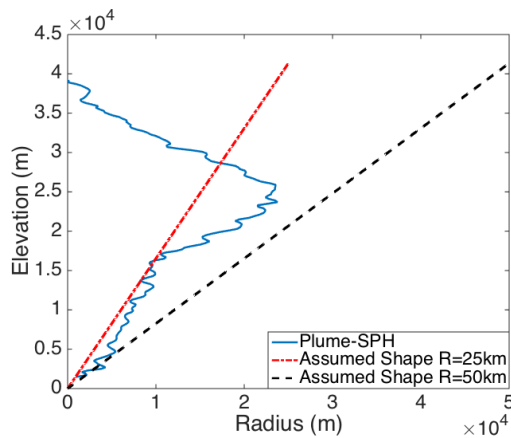


Figure 13. Comparison between radius of initial ash clouds created by 3D plume model (Plume-SPH) and assumed initial ash cloud shape in Puff. The plume shape expression used in Puff defines an inverted cone whose actual shape changes when “horizontal spread” takes different values. $R = 25\text{km}$ is corresponding to “horizontal spread” equals to 50km . $R = 50\text{km}$ is corresponding to “horizontal spread” equals to 100km

Comparison between cross-sectional views of the initial ash clouds is shown in Fig. 14. The cross-sectional view of assumed plume shape (last figure in Fig. 14) is similar to cross-sectional view of simulated 3D plume in general sense. However, for simulated 3D plume, the ash particle distribution on cross section varies along with height. It is

hard for semiempirical expressions have such feature. In Puff, particle distribution on cross sections is assumed to be the same.

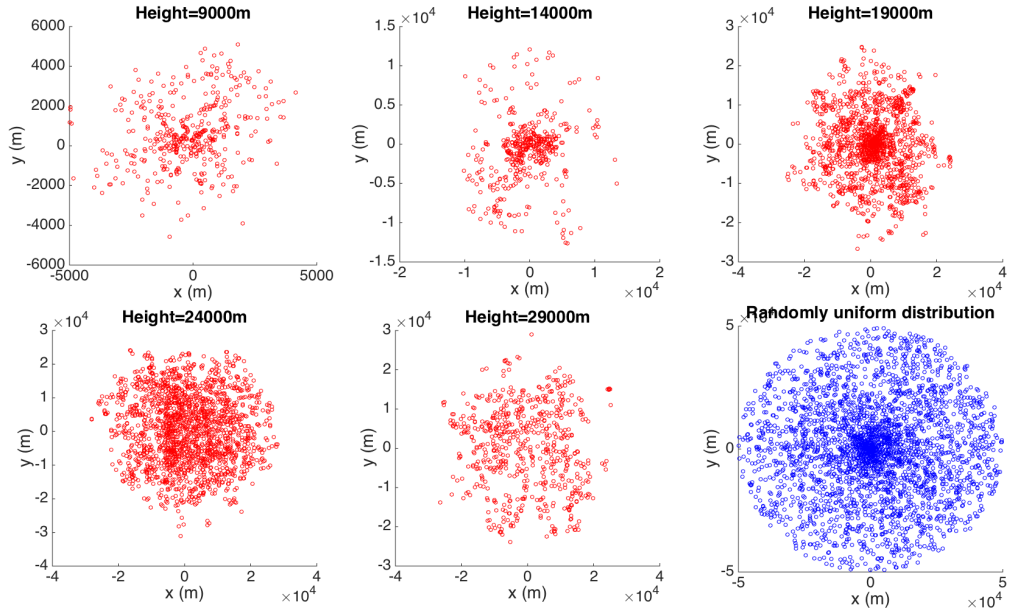


Figure 14. Horizontal distribution of ash particles (tracers) on a cross section of initial ash cloud. Puff assumes randomly uniform distribution of ash particle within a circle, as shown by blue dots in the last figure. All other figures show ash particle distribution of initial ash cloud created by Plume-SPH at different elevations.

Assigning different values to “horizontal spread” has ignorable effect on VATD simulation results. We use numbers between 50km to 1600km as “horizontal spread” to create initial ash cloud for VATD, all of them generate very similar results. Figure 15 shows two different simulation results based on initial ash cloud with “horizontal spread” equals to 50km and 600km respectively. No visible differences can be told between them. This implies that horizontal distribution has less significant influence on VATD simulation results than vertical distribution.

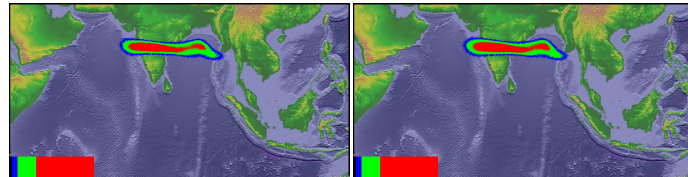


Figure 15. Ash transportation simulated by Puff at around 55 hours after eruption (UT 199106171141). Different values for “horizontal spread” are used to create initial ash cloud. Pictures to the left is corresponding to “horizontal spread” equals to 50kmm . Pictures to the right is corresponding to “horizontal spread” equals to 600kmm . The observed cloud image is in Fig. 7.

4 Conclusion

This paper presented, for the first time, VATD simulations using intial conditions created by a 3D plume model. Traditional VATD simulations use initial conditions cre-

530 ated according to a semiempirical plume shape expression. A case study of the 1991 Pinatubo
 531 eruption demonstrates that a 3D plume model can create more realistic initial ash cloud
 532 and ash parcel positions, and therefore improve the accuracy of ash transport forecasts.
 533 Informal sensitivity analyses suggest that initial conditions, as expressed in the dispo-
 534 sition of initial ash parcel positions in the vertical, have a more significant effect on a vol-
 535 canic ash transport forecast than most other parameters. Comparison of initial ash par-
 536 cel distributions among the 3D plume model, semiempirical expressions, and observa-
 537 tions suggests that a major subpopulation of ash parcels should be placed at a much lower
 538 elevation than maximum height to obtain a better VATD forecast. For the Pinatubo case
 539 study, “well-matched” simulation results are observed when using a maximum height of
 540 around 30km, which is much lower than the observed maximum height of 40km. Com-
 541 paring the effects of the maximum height, vertical spread and horizontal spread shows
 542 that ash particle distribution in the vertical direction has the strongest effect on VATD
 543 simulation.

544 We have presented a novel method for creating *a priori* initial conditions for VATD
 545 simulations. We have shown that it might be possible to obtain initial positions of ash
 546 parcels with deterministic forward modeling of the volcanic plume, obviating the need
 547 to attempt to obtain initial positions or a history of release heights via inversion (?). Al-
 548 though the method now suffers from the high computational cost associated with 3D for-
 549 ward modeling, it not only helps overcome shortcomings of existing methods used to gen-
 550 erate *a priori* input parameters, but also overcomes the need to do the thousands of runs
 551 associated with inverse modeling. In addition, computational cost will continue to di-
 552 minish as computing speed increases. As they are forward numerical models based on
 553 first principles, 3D plume models need little if any parameterization, and user interven-
 554 tion should not be required to improve forecast power; no assumption about the initial
 555 position of ash parcels is needed. Generation of the initial cloud of ash parcels directly
 556 by 3D simulation is potentially adaptable to a variety of volcanic and atmospheric sce-
 557 narios. In contrast, semiempirical expressions used to determine initial conditions require
 558 several parameters to control ash particle distribution along a vertical line source or some
 559 simplified shape of the initial ash cloud, making it difficult in some cases to generate ini-
 560 tial conditions that closely resemble a complex reality.

561 The full range of research issues raised by numerical forecasting of volcanic clouds
 562 is diverse. We described in this paper the effect of initial conditions chosen from the out-
 563 put of a 3D plume model on numerical forecasts of volcanic ash transport simulation.
 564 The wind field, another important factor in volcanic ash transportation simulation is not
 565 discussed in the present work. Some other aspects, such as small scale physical processes,
 566 even though they play lesser roles, might need to be included in VATDs to improve ac-
 567 curacy for a particular eruption. In addition, eruption conditions are subject to change
 568 with time, even during the climactic phase of an eruption. In the future, time-dependent
 569 initial conditions for VATDs can be created from 3D plume simulations with time-dependent
 570 eruption conditions.

571 **Acknowledgments**

572 Support for the Twentieth Century Reanalysis Project dataset is provided by the U.S.
 573 Department of Energy, Office of Science Innovative and Novel Computational Impact
 574 on Theory and Experiment (DOE INCITE) program, and Office of Biological and En-
 575 vironmental Research (BER), and by the National Oceanic and Atmospheric Adminis-
 576 tration Climate Program Office.

577 **References**

- 578 Avdyushin, S., Tulinov, G., Ivanov, M., Kuzmenko, B., Mezhuev, I., Nardi, B., ...
 579 Chanin, M.-L. (1993). 1. spatial and temporal evolution of the optical thick-

- ness of the pinatubo aerosol cloud in the northern hemisphere from a network of ship-borne and stationary lidars. *Geophysical research letters*, 20(18), 1963–1966.
- Bonadonna, C., & Houghton, B. (2005). Total grain-size distribution and volume of tephra-fall deposits. *Bulletin of Volcanology*, 67(5), 441–456.
- Bursik, M. (2001). Effect of wind on the rise height of volcanic plumes. *Geophys. Res. Lett.*, 28(18), 3621–3624.
- Bursik, M., Jones, M., Carn, S., Dean, K., Patra, A., Pavolonis, M., ... others (2012). Estimation and propagation of volcanic source parameter uncertainty in an ash transport and dispersal model: application to the eyjafjallajokull plume of 14–16 april 2010. *Bulletin of volcanology*, 74(10), 2321–2338.
- Cao, Z., Patra, A., Bursik, M., Pitman, E. B., & Jones, M. (2018). Plume-sph 1.0: a three-dimensional, dusty-gas volcanic plume model based on smoothed particle hydrodynamics. *Geoscientific Model Development*, 11(7), 2691–2715.
- Cerminara, M., Esposti Ongaro, T., & Berselli, L. (2016). Ashee-1.0: a compressible, equilibrium-eulerian model for volcanic ash plumes. *Geoscientific Model Development*, 9(2), 697–730.
- Cerminara, M., Esposti Ongaro, T., & Neri, A. (2016). Large eddy simulation of gas-particle kinematic decoupling and turbulent entrainment in volcanic plumes. *Journal of Volcanology and Geothermal Research*.
- Compo, G. P., Whitaker, J. S., & Sardeshmukh, P. D. (2006). Feasibility of a 100-year reanalysis using only surface pressure data. *Bulletin of the American Meteorological Society*, 87(2), 175–190.
- Compo, G. P., Whitaker, J. S., Sardeshmukh, P. D., Matsui, N., Allan, R. J., Yin, X., ... others (2011). The twentieth century reanalysis project. *Quarterly Journal of the Royal Meteorological Society*, 137(654), 1–28.
- Costa, A., Suzuki, Y., Cerminara, M., Devenish, B., Esposti Ongaro, T., Herzog, M., ... others (2016). Results of the eruptive column model inter-comparison study. *Journal of Volcanology and Geothermal Research*.
- Daniele, P., Lirer, L., Petrosino, P., Spinelli, N., & Peterson, R. (2009). Applications of the puff model to forecasts of volcanic clouds dispersal from etna and vesuvio. *Computers & Geosciences*, 35(5), 1035–1049.
- DeFoor, T. E., Robinson, E., & Ryan, S. (1992). Early lidar observations of the june 1991 pinatubo eruption plume at mauna loa observatory, hawaii. *Geophysical research letters*, 19(2), 187–190.
- Degruyter, W., & Bonadonna, C. (2012). Improving on mass flow rate estimates of volcanic eruptions. *Geophysical Research Letters*, 39(16).
- de'Michieli Vitturi, M., Neri, A., & Barsotti, S. (2015). Plume-mom 1.0: A new integral model of volcanic plumes based on the method of moments. *Geoscientific Model Development*, 8(8), 2447–2463.
- Deshler, T., Hofmann, D., Johnson, B., & Rozier, W. (1992). Balloonborne measurements of the pinatubo aerosol size distribution and volatility at laramie, wyoming during the summer of 1991. *Geophysical research letters*, 19(2), 199–202.
- Devenish, B. (2013). Using simple plume models to refine the source mass flux of volcanic eruptions according to atmospheric conditions. *Journal of Volcanology and Geothermal Research*, 256, 118–127.
- Draxler, R. R., & Hess, G. (1998). An overview of the hysplit_4 modelling system for trajectories. *Australian meteorological magazine*, 47(4), 295–308.
- D'amours, R. (1998). Modeling the etex plume dispersion with the canadian emergency response model. *Atmospheric Environment*, 32(24), 4335–4341.
- Fero, J., Carey, S. N., & Merrill, J. T. (2008). Simulation of the 1980 eruption of mount st. helens using the ash-tracking model puff. *Journal of Volcanology and Geothermal Research*, 175(3), 355–366.
- Fero, J., Carey, S. N., & Merrill, J. T. (2009). Simulating the dispersal of tephra from the 1991 pinatubo eruption: implications for the formation of widespread ash

- 634 layers. *Journal of Volcanology and Geothermal Research*, 186(1), 120–131.
- 635 Folch, A., Costa, A., & Macedonio, G. (2009). Fall3d: A computational model for
636 transport and deposition of volcanic ash. *Computers & Geosciences*, 35(6), 1334–
637 1342.
- 638 Folch, A., Costa, A., & Macedonio, G. (2016). Fplume-1.0: An integral volcanic
639 plume model accounting for ash aggregation. *Geoscientific Model Development*,
640 9(1), 431.
- 641 Guo, S., Bluth, G. J., Rose, W. I., Watson, I. M., & Prata, A. (2004). Re-evaluation
642 of so₂ release of the 15 june 1991 pinatubo eruption using ultraviolet and infrared
643 satellite sensors. *Geochemistry, Geophysics, Geosystems*, 5(4).
- 644 Guo, S., Rose, W. I., Bluth, G. J., & Watson, I. M. (2004). Particles in the great
645 pinatubo volcanic cloud of june 1991: The role of ice. *Geochemistry, Geophysics,
646 Geosystems*, 5(5).
- 647 Holasek, R., Self, S., & Woods, A. (1996). Satellite observations and interpretation
648 of the 1991 mount pinatubo eruption plumes. *Journal of Geophysical Research:
649 Solid Earth*, 101(B12), 27635–27655.
- 650 Holasek, R. E., Woods, A. W., & Self, S. (1996). Experiments on gas-ash separation
651 processes in volcanic umbrella plumes. *Journal of volcanology and geothermal re-
652 search*, 70(3-4), 169–181.
- 653 Jäger, H. (1992). The pinatubo eruption cloud observed by lidar at garmisch-
654 partenkirchen. *Geophysical research letters*, 19(2), 191–194.
- 655 Mastin, L. G. (2007). A user-friendly one-dimensional model for wet volcanic
656 plumes. *Geochemistry, Geophysics, Geosystems*, 8(3).
- 657 Neri, A., Esposti Ongaro, T., Macedonio, G., & Gidaspow, D. (2003). Multiparticle
658 simulation of collapsing volcanic columns and pyroclastic flow. *Journal of Geo-
659 physical Research: Solid Earth (1978–2012)*, 108(B4).
- 660 Oberhuber, J. M., Herzog, M., Graf, H.-F., & Schwanke, K. (1998). Volcanic plume
661 simulation on large scales. *Journal of Volcanology and Geothermal Research*,
662 87(1), 29–53.
- 663 Paladio-Melosantos, M. L. O., Solidum, R. U., Scott, W. E., Quiambao, R. B., Um-
664 bal, J. V., Rodolfo, K. S., ... Ruelo, H. B. (1996). Tephra falls of the 1991
665 eruptions of mount pinatubo. *Fire and mud*, 12000, 12030.
- 666 Pouget, S., Bursik, M., Singla, P., & Singh, T. (2016). Sensitivity analysis of a one-
667 dimensional model of a volcanic plume with particle fallout and collapse behavior.
668 *Journal of Volcanology and Geothermal Research*.
- 669 Schwaiger, H. F., Denlinger, R. P., & Mastin, L. G. (2012). Ash3d: A finite-volume,
670 conservative numerical model for ash transport and tephra deposition. *Journal of
671 Geophysical Research: Solid Earth*, 117(B4).
- 672 Scott, W. E., Hoblitt, R. P., Torres, R. C., Self, S., Martinez, M. M. L., & Nillos,
673 T. (1996). Pyroclastic flows of the june 15, 1991, climactic eruption of mount
674 pinatubo. *Fire and Mud: eruptions and lahars of Mount Pinatubo, Philippines*,
675 545–570.
- 676 Searcy, C., Dean, K., & Stringer, W. (1998). Puff: A volcanic ash tracking and pre-
677 diction model. *Journal of Volcanology and Geothermal Research*, 80, 1–16.
- 678 Self, S., Zhao, J.-X., Holasek, R. E., Torres, R. C., & King, A. J. (1996). The atmo-
679 pheric impact of the 1991 mount pinatubo eruption.
- 680 Stefanescu, E., Patra, A., Bursik, M., Madankan, R., Pouget, S., Jones, M., ...
681 others (2014). Temporal, probabilistic mapping of ash clouds using wind field
682 stochastic variability and uncertain eruption source parameters: Example of the
683 14 april 2010 eyjafjallajökull eruption. *Journal of Advances in Modeling Earth
684 Systems*, 6(4), 1173–1184.
- 685 Suzuki, T., et al. (1983). A theoretical model for dispersion of tephra. *Arc volca-
686 nism: physics and tectonics*, 95, 113.
- 687 Suzuki, Y., & Koyaguchi, T. (2009). A three-dimensional numerical simulation of

- 688 spreading umbrella clouds. *Journal of Geophysical Research: Solid Earth* (1978–
689 2012), 114(B3).
- 690 Suzuki, Y. J., Koyaguchi, T., Ogawa, M., & Hachisu, I. (2005). A numerical study
691 of turbulent mixing in eruption clouds using a three-dimensional fluid dynamics
692 model. *Journal of Geophysical Research: Solid Earth*, 110(B8).
- 693 Tanaka, H. (1991). Development of a prediction scheme for the volcanic ash fall
694 from redoubt volcano. In *First int'l. symp. on volcanic ash and aviation safety*
695 (Vol. 58).
- 696 Walko, R., Tremback, C., & Bell, M. (1995). Hypact: The hybrid particle and con-
697 centration transport model. *User's guide*.
- 698 Whitaker, J. S., Compo, G. P., Wei, X., & Hamill, T. M. (2004). Reanalysis without
699 radiosondes using ensemble data assimilation. *Monthly Weather Review*, 132(5),
700 1190–1200.
- 701 Witham, C., Hort, M., Potts, R., Servranckx, R., Husson, P., & Bonnardot, F.
702 (2007). Comparison of vaac atmospheric dispersion models using the 1 november
703 2004 grimsvötn eruption. *Meteorological Applications*, 14(1), 27–38.
- 704 Woodhouse, M., Hogg, A., Phillips, J., & Sparks, R. (2013). Interaction between vol-
705 canic plumes and wind during the 2010 eyjafjallajökull eruption, iceland. *Journal*
706 *of Geophysical Research: Solid Earth*, 118(1), 92–109.
- 707 Woods, A. (1988). The fluid dynamics and thermodynamics of eruption columns.
708 *Bulletin of Volcanology*, 50(3), 169–193.
- 709 Zidikheri, M. J., Lucas, C., & Potts, R. J. (2017). Estimation of optimal dispersion
710 model source parameters using satellite detections of volcanic ash. *Journal of Geo-
711 physical Research: Atmospheres*, 122(15), 8207–8232.